J Forensic Sci, May 2006, Vol. 51, No. 3
doi:10.1111/j.1556-4029.2006.00111.x
Available online at: www.blackwell-synergy.com

Donato Firrao,[1] M.Sc.; Paolo Matteis,[1] Ph.D.; Giorgio Scavino,[1] Laurea; Graziano Ubertalli,[1] Laurea; Maria G. Ienco,[2] Laurea; Gabriella Pellati,[2] Laurea; Paolo Piccardo,[2] Ph.D.; Maria R. Pinasco,[2] Laurea; Enrica Stagno,[2] Laurea; Girolamo Costanza,[3] Ph.D.; Roberto Montanari,[3] Laurea; Maria E. Tata,[3] Ph.D.; Giovanni Brandimarte,[4] Laurea; and Santo Petralia,[4] Laurea

Metal Objects Mapping After Small Charge Explosions. A Study on AISI 304Cu Steel with Two Different Grain Sizes

ABSTRACT: Evidence of exposure of a metal component to a small charge explosion can be detected by observing microstructural modifications; they may be present even if the piece does not show noticeable overall plastic deformations. Particularly, if an austenitic stainless steel (or another metal having a face-centered cubic structure and a low stacking fault energy) is exposed to an explosive shock wave, high-speed deformation induces primarily mechanical twinning, whereas, in nonexplosive events, a lower velocity plastic deformation first induces slip. The occurrence of mechanical twins can be detected even if the surface is damaged or oxidized in successive events. In the present research, optical metallography (OM) and scanning electron microscopy (SEM), and scanning tunneling microscopy (STM) were used to detect microstructural modifications caused on AISI 304Cu steel disks by small-charge explosions. Spherical charges of 54.5 or 109 g TNT equivalent mass were used at explosive-to-target distances from 6.5 to 81.5 cm, achieving peak pressures from 160 to 0.5 MPa. Explosions induced limited or no macro-deformation. Two alloy grain sizes were tested. Surface OM and SEM evidenced partial surface melting, zones with recrystallization phenomena, and intense mechanical twinning, which was also detected by STM and X-ray diffraction. In the samples' interior, only twins were seen, up to some distance from the explosion impinged surface and again, at the shortest charge-to-sample distances, in a thin layer around the reflecting surface. For forensic science locating purposes after explosions, the maximum charge-to-target distance at which the phenomena disappear was singled out for each charge or grain size and related to the critical resolved shear stress for twinning.

KEYWORDS: forensic science, explosion, shock wave, stainless steel, mechanical twinning, optical microscopy, scanning electron microscopy, scanning tunneling microscopy, X-ray diffraction

Metal object mapping after an explosion is an important issue in forensic science. After an explosion, various effects can be observed in a metal target, namely fracture, gross and localized plastic deformation, surface modifications of various kinds, and microstructural crystallographic alterations with ensuing changes in mechanical properties (1,2). At some distance from an explosive charge, macro effects disappear; only microstructural variations, such as recrystallization phenomena, intense slip bands and/or mechanical twins, possible phase transformations are present, with the former to disappear first as distance increases. In the case of small charge explosions, macro effects are restricted to very small charge-to-target distances (of the order of a few centimeters), with most of the variations being of the crystal alteration type; no macro-deformation is detectable for distances above 10–20 cm. Thus, mapping is difficult and objects launched far away may not be identified as associated with the explosion event.

If another damaging event follows, such as in an explosion in an aircraft that subsequently crashes, the macro features of a small charge explosion can be obscured and the explosion ruled out. Yet, crystal micro modifications (intense slip bands or mechanical twinning) characteristic of an explosion are still present and can prove the fact even after many years, or even if corrosion processes have obliterated the surface features (1). Moreover, mechanical twinning without slip is often the unique feature in the case of high-velocity deformations ($>10^4$/s (3)).

Competition between slip and twins is decided by the value of the stacking fault energy (γ_{sf}) of the metals undergoing explosive shocks. In the literature, there is no reference to the maximum distance from the explosion center at which explosion effects (macrodeformation, microdeformation, crystal structure alterations, etc.) can still be detected. Calculations of the shear stress arising from the overpressure at such a threshold can be attempted using elasticity theory formulations (3) and results compared with the minimum shear stress necessary to form slip bands or twins (1). Yet, experimental proofs of the validity of the approach do not exist.

A comprehensive experimental program has been undertaken to investigate the relationship between relevant shock wave parameters and microstructural effects that can be observed in a metal target undergoing an explosion. Disks made of several face-centered cubic (FCC) metals chosen from low to high γ_{sf} values were used as targets. Results of the first series of experiments on AISI 304Cu specimens undergoing explosions at various distances are presented. This steel was selected because studies on a steel of similar composition have shown that it has a limited tendency to form ε-martensite, which could yield conflicting results (4). Explosion overpressure measurements with sensors at various charge-to-target distances have also been performed.

[1]Dip. di Sc. dei Materiali ed Ing. Chimica, Politecnico di Torino, Torino, Italy.
[2]Dip. di Chimica e Chimica Industriale, Università di Genova, Genova, Italy.
[3]Dip. di Ing. Meccanica, Università di Roma Tor Vergata, Roma, Italy.
[4]Marina Militare, Istituto Chimica Esplosivi, Mariperman, La Spezia, Italy.

Received 10 Feb. 2005; and in revised form 6 Aug. 2005, 13 Nov. 2005; accepted 13 Nov. 2005; published 5 April 2006.

TABLE 1—*AISI 304Cu stainless-steel analysis (wt%).*

C	S	P	Si	Mn	Cr	Ni	Mo	Cu	N
0.015	0.001	0.023	0.41	0.88	17.26	9.16	0.24	3.44	0.017

Methods and Results

Specimen Preparation

Two series of disk-shaped specimens have been produced, each series being characterized by a distinct grain size. Preparation assured the absence of those microstructural characteristics, such as mechanical twins and slip bands, that the successive explosions could produce. AISI 304Cu (EN 1.4567/X 3 CrNiCu 18-9) bars having the composition reported in Table 1 were used, and samples were fabricated adopting the following steps:

- solution heat-treatment of the bars at 1060°C and 1200°C, respectively, in order to obtain two different grain sizes;
- cutting of the disks and first polishing with 60 grit abrasive papers;
- stress relieving at 1050°C for 4 h, with successive cooling in nitrogen;
- permanent marking;
- mechanical polishing (of the unmarked face) with 80–1000 grit abrasive papers; and
- electrolytic preparation of the central part (about 2 cm^2) of the same face, by polishing with Struers A2 reactant and 1 min etching with 10% oxalic acid.

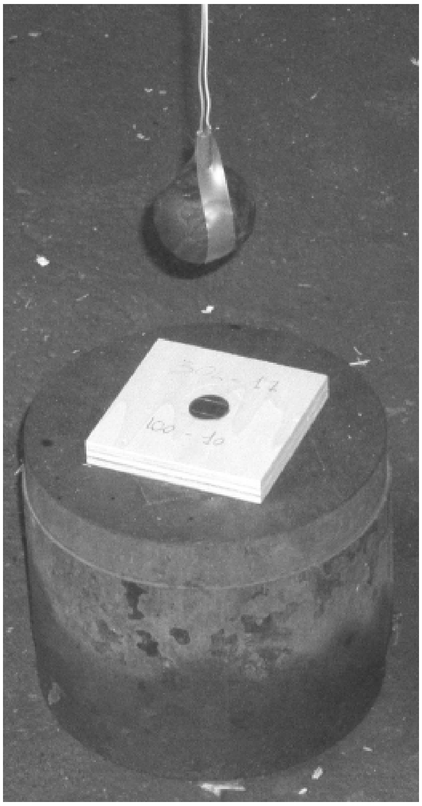

FIG. 1—*View of experimental setups with AISI 304Cu specimens.*

Experimental Setups

The experimental setups are shown in Figs. 1 and 2. Spherical unconfined charges, consisting of either 50 or 100 g of plastic explosive NSP Bofors Nobelkrut D UN N.0084 (Table 2), were detonated in the "P. Cottrau" Italian Navy Proving Ground by cylindrical detonators inserted at their cores; spheres were hung from detonator electrical cables. TNT equivalence was experimentally determined through the ballistic pendulum as 1.09 mass units of TNT per mass unit of the explosive used. TNT equivalents of the charges were 54.5 and 109 g, respectively. The specimens' polished and etched surfaces, as well as the pressure sensor surfaces, were placed horizontally below the charges. Blast waves could be approximated as plane waves considering distances and specimens' dimensions; such an approximation may not be completely valid at the shortest distances.

To approximate free-surface condition on the face not directly exposed to the shock wave, specimens were supported only by a very thin circumferential rim of the wooden specimen holders. Destruction of the holders at all distances (except in a few cases at the largest distances) proved that all the specimens can be considered as unconstrained (Fig. 3). Specimens were found either inside the steel mortar or on the ground in the vicinity of the experimental setup. Secondary impacts of some specimens against the mortar's inner wall may have occurred. Although in most specimens evidences of secondary impacts were not found, the successive observations were restricted to the central polished part, away from the edges.

The pressure sensors (Kistler PCB 102A type) were bonded to a steel adaptor screwed to a lead support to damp the shock wave when it passes the sensor, thus reducing reflections. The charge-to-sample distances, *d*, between the center of the prepared spherical charges (3 and 4 cm diameter for 50 and 100 g charges,

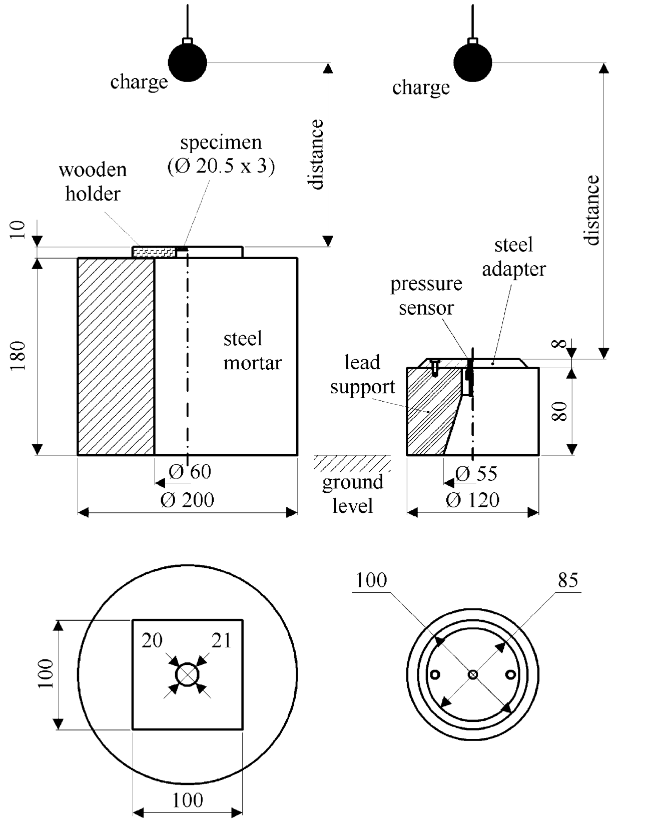

FIG. 2—*Drawing of experimental setups with AISI 304Cu specimens (left) and with pressure sensors (right); dimensions in mm.*

TABLE 2—*Chemical analysis of the explosive (wt%).*

(Measures by extraction)			(Measure from calcined residual)
Pentrite $C_5H_8N_4O_{12}$	Plasticizer	Polymer	Carbon Black
86	11	2	0.45

respectively) and the specimen upper surface were in the 6.5–81.5 cm range.

Specimen Deformation

The disk thickness was not modified by the explosions, except for specimens very close to the charges, which showed either a slight decrease owing to compression (50 g charges), or a slight increase owing to melting of large portions of the surfaces (100 g). At charge-to-specimen distances larger than 10 cm (50 g explosive charges) or 18 cm (100 g charges), no macroscopic deformation was detected, thus revealing that general yielding was not reached. Therefore, at distances above these limits, elasticity theory can be applied to transform surface overpressures into surface applied shear stresses (1,3).

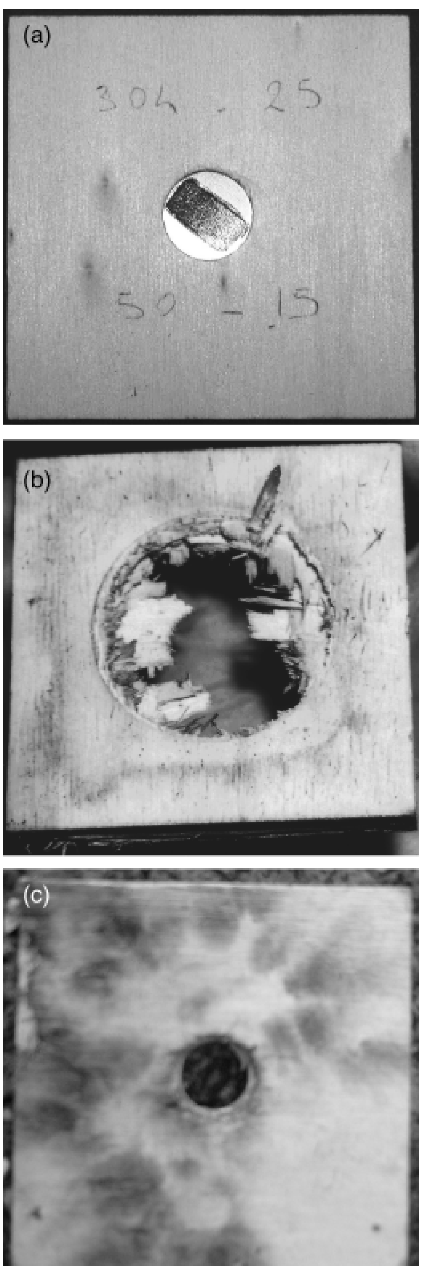

FIG. 3—*Specimen-holders: ready with mounted specimen (a), after explosions at intermediate (b) and large (c) distance.*

Explosion Gases Overpressure

The maximum free-field overpressure (p_d) resulting from the explosion of a spherical charge at a given reduced distance (defined as $r = dm^{-1/3}$, where m is the charge's TNT equivalent mass) can be estimated by the following semi-empirical formulas by Henrych (5), where the pressures and the reduced distances are expressed in kgf/cm^2 and in m/kg$^{1/3}$, respectively.

$$\begin{aligned} p_d - p_0 &= \frac{14.0717}{r} + \frac{5.5397}{r^2} - \frac{0.3572}{r^3} + \frac{0.00625}{r^4} \quad (0.05 \le r \le 0.3) \\ p_d - p_0 &= \frac{6.1938}{r} - \frac{0.3262}{r^2} + \frac{2.1324}{r^3} \quad (0.3 \le r \le 1) \\ p_d - p_0 &= \frac{0.662}{r} + \frac{4.05}{r^2} + \frac{3.288}{r^3} \quad (1 \le r \le 10) \end{aligned} \tag{1}$$

The overpressure exercised by the explosion gases (mixed with air) upon the exposed surface (p_r), usually defined as reflected pressure, is nevertheless higher than the same gases' free-field pressure, because the presence of the specimen surface hinders gas expansion. p_d and p_r at the same distance can be related through p_0, the ambient pressure, by a further correlation (6):

$$\frac{p_r}{p_d} = 2 + \frac{6(p_d/p_0)}{(p_d/p_0) + 7} \tag{2}$$

The p_r estimate obtained through the combined use of Eq. 1 and of Eq. 2 may not be sufficiently approximated, because they have been obtained from experiments performed, in the majority of cases, under conditions significantly different from the ones adopted in the present series of explosions, where much smaller charges and distances were selected. Nevertheless, more recently published free-field overpressure measurements (7,8), while resulting in values close to those that can be obtained using Henrych's formulas, signal lower mean values in the 0.3 to 1 m/kg$^{-1/3}$ reduced distance range. Also, these experiments were performed with charges (200–590 g) and distances (0.2–7 m) rather large with respect to the present study.

Thus, in order to obtain an estimate of the reflected overpressure under conditions similar to the present experiments, 22 instrumented explosions were performed at distances in the 11.5–33.5 cm range with 50 g charges and in the 17–37 cm range with 100 g charges, obtaining measured overpressures in the 11–45 MPa range. The peak overpressure and the rise time were obtained from recorded pressure–time curves (0.1 μs sampling). In Fig. 4, all experimental peak overpressures are presented as a function of r; the resulting interpolation curve is different from the curve computed as described before and is considered more precise for the small distances and charges used in the present work. Hence, overpressure values for explosion-subjected specimens were calculated from the obtained interpolation expression, namely

$$p_r = 13.37/r + 0.141/r^2 \quad (0.3 \le r \le 0.88) \tag{3}$$

where p_r and r are expressed in MPa and in m/kg$^{1/3}$, respectively.

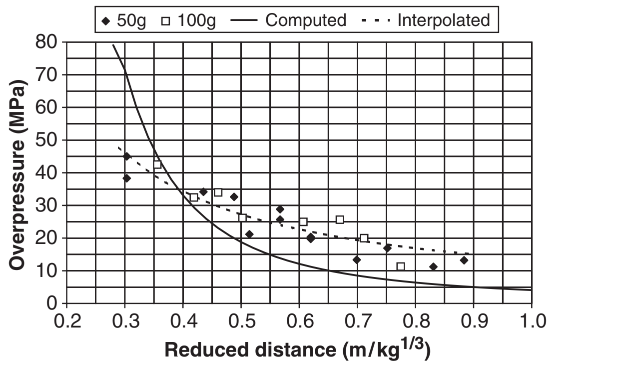

FIG. 4—*Measured, computed (from Eqs. 1 and 2) and interpolated (present results, Eq. 3) peak reflected overpressures as a function of r.*

The overpressure rise times ranged from 4 to 19 μs (on average longer for shorter distances), much longer than the time needed for the shock wave to travel to the specimen's opposite face (calculated as about 0.5 μs for an elastic uniaxial-deformation wave, by considering the steel's density and elastic modulus (9)).

Stresses Inside the Specimen

In FCC metals exposed to small-charge explosions, plastic deformations appear mainly as twinning phenomena inside crystals (1), due to the local maximum shear stress reaching a critical value. Under conditions of no gross plastic deformation, if mechanical twins (or slips) occur only inside isolated grains, it means that the general yielding condition has not been reached; thus it has been hypothesized that, under conditions near to the detectable threshold of permanent modifications in the metal, the elasticity theory could be applied. This hypothesis is confirmed by the fact that over certain charge-to-target distances, macroscopic deformation (and thus generalized yielding) was not observed.

Meyers and Chawla (3) indicate that, using the elastic uniaxial deformation hypothesis, the maximum shear stress τ_{max} inside a metal impinged by a pressure $p = p_r$ results from the expression

$$\tau_{max} = \frac{3(1-2\nu)}{2(1+\nu)} p_r \tag{4}$$

where ν is the Poisson's ratio (0.28 for the steel used (9)).

The shock-wave propagation inside the specimen occurs with a gradual damping of its maximum pressure value, and thus of the corresponding maximum shear stress.

From data obtained in the experimental instrumented explosions (Eq. 3) and applying the elasticity theory (Eq. 4) when the charge-to-target distance is higher than 10 and 18 cm, respectively, in the 50 and 100 g charge tests, the maximum shear stress τ_{max} at the specimen's surface can be obtained as a function of the distance for each used charge (Fig. 5).

Microstructures

The original microstructure showed polygonal grains with frequent large recrystallization twins; precipitates (or cavities subsequent to their extraction) were observed along polygonal boundaries, but not along twin boundaries (Fig. 6). The two groups of specimens exhibited 60- and 32-μm grain sizes after annealing at 1200°C and 1060°C, respectively.

The surface modifications observed after blast by optical metallography (OM) and scanning electronic microscopy (SEM), in

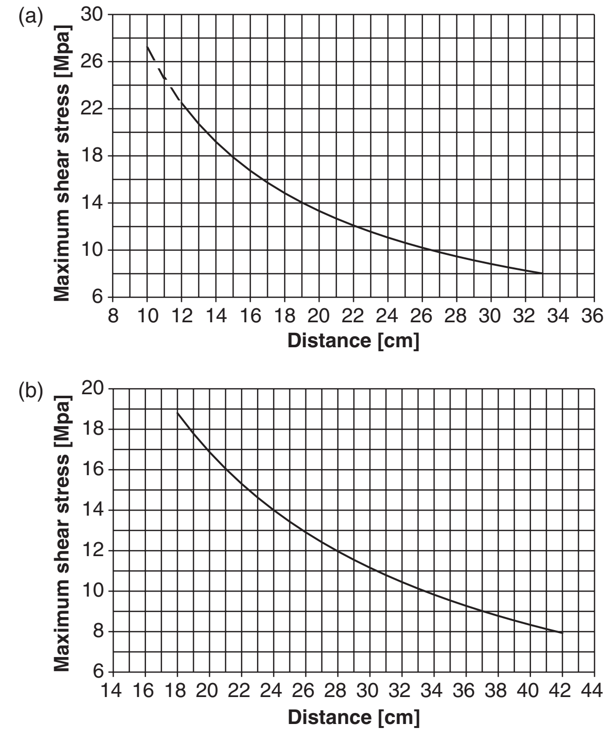

FIG. 5—*Maximum shear stress, τ_{max}, at the specimens' surface as a function of the charge-to-target distance when gross deformation disappears (from Eq. 3 and Eq. 4); (a) 50 g NSP charge, (b) 100 g NSP charge.*

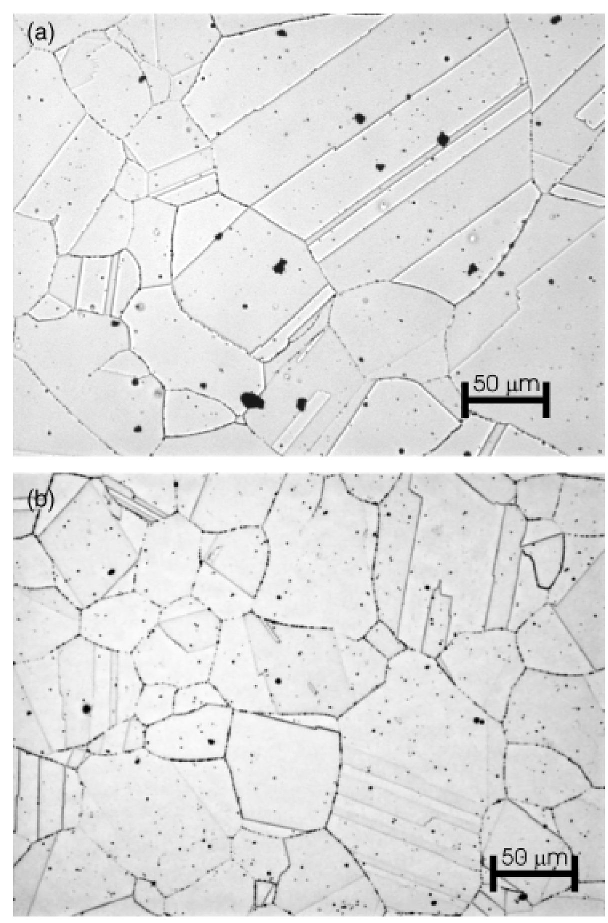

FIG. 6—*Original microstructure of AISI 304Cu stainless steel; large-grain (60 μm, a) and small-grain (32 μm, b) samples.*

different cases, include dark spots owing to deposition of oxidized explosive components, deposits of material originated from detonator case fragments, large area fusion and subsequent oxidation, partial melting (at grain boundaries), and mechanical twins. The modifications observed in the metallographic sections perpendicular to the exposed surfaces, obtained by electrical discharge machining (EDM), were restricted to mechanical twins only. The mechanical twins were much more evident through the OM than

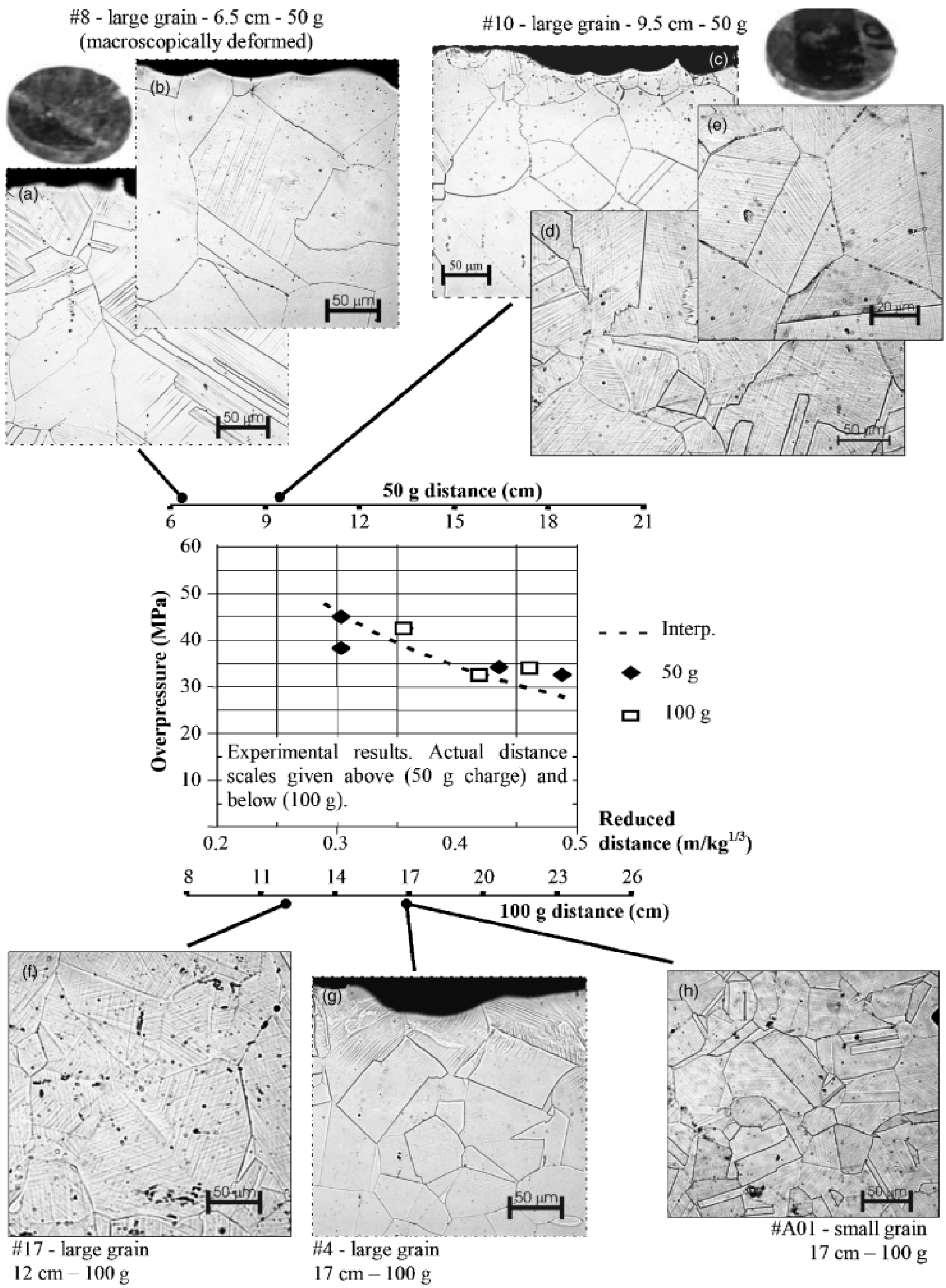

FIG. 7—*Microstructural modifications in blast-exposed specimens at various points of the experimental overpressure–distance curve; reduced distance in the 0.2–0.5 m/kg*$^{1/3}$ *range.*

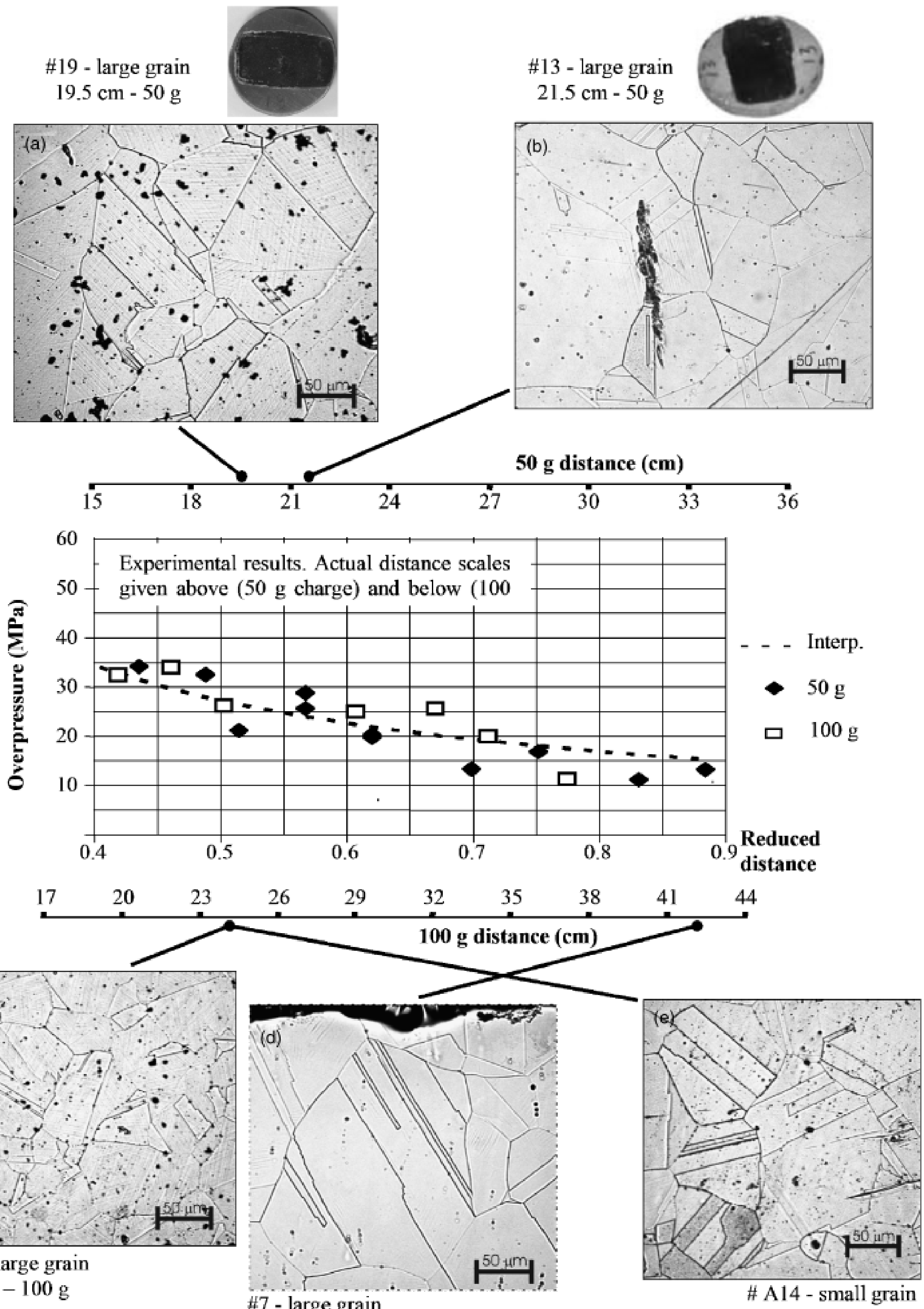

FIG. 8—*Microstructural observations of exposed specimens as in Fig. 7; reduced distances in the 0.4–0.9 m/kg$^{1/3}$ range.*

through the SEM, particularly for those observed on the cross sections.

It should be noted that the modifications identified as mechanical twins upon the blast-exposed surfaces are planarity variations of the original polished and etched surface directly owing to the shock wave, whereas, on the perpendicular sections, the analogous planarity variations are owing to the metallographic etch performed after the explosions and, thus, depend also on the etch intensity. For this reason, only the exposed surfaces were observed through scanning tunneling microscopy (STM) to gather informa-

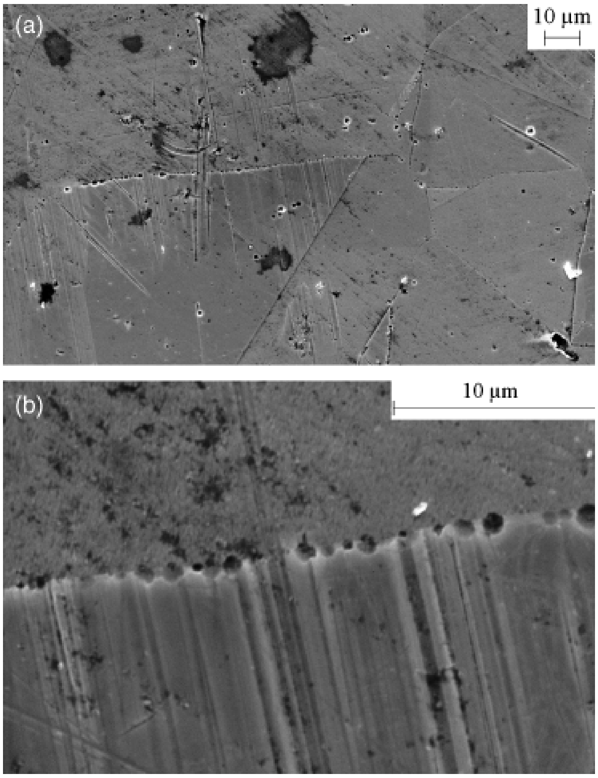

FIG. 9—*Scanning electron microscopy images of exposed surface of sample #2 , 50 g charge, 13.5 cm distance; artifacts (scratches) attributed to contacts with gravel on the ground after the explosion.*

tion not dependent on postexplosions etching. A larger collection of optical micrographs of blast exposed samples can be found in Ref. (10).

The importance of the reduced distance in controlling the occurrence of microstructural changes is clearly demonstrated by Fig. 7, where surface and cross-section modifications are grouped for the smallest values of r computed with both charges, and Fig. 8, where the analogous features are reported for the largest r's.

As regards the specimens at the lowest charge-to-target distances, it can be seen that intense mechanical twinning occupies all of the exposed surface, as well as of the grains inside a discontinuous layer adjacent to the surface in the cross section, both in the large grain series (Fig. 7*a–e* with 50 g charge and Fig. 7*f* and *g* with 100 g charge) and in the small grain series (Fig. 7*h*). The closest specimens to the charge have exposed surfaces too ruined to yield clear pictures. A few isolated slips were observed upon the exposed surfaces of large-grain specimens number 8 and 17, exposed to the maximum pressures. In specimens at the smallest distance, the twinned layer in the section was limited to the central zone of the exposed surface (Fig. 7*a* and *b*); at higher distances, the same layer showed random discontinuities. Alignments of much smaller recrystallization grains were observed in isolated areas of the section, near the exposed border, of the specimen at the 9.5 cm distance in the large grain, 50 g charge series (Fig. 7*c*). As these smaller grains are free of mechanical twins, the overpressure wave had already passed when their formation was completed. The lack of small grains, or of grains free from twins in the section of the corresponding specimen at the 6.5 cm distance, may indicate that the overtemperature wave was much more intense in this case (partial fusion occured on the surface) and grain growth occurred; the overpressure wave still had time to cause twins in the new grains after grain growth ended.

Comparing Fig. 8*a* and *b* (50 g charge, large grain series) and Fig. 8*c* and *d* (100 g charge, large grain series), with corresponding pictures in Fig. 7, it can be seen that, upon increasing the distance, mechanical twins were gradually less evident (Fig. 8*a* and *c*) and finally either limited to areas around fragment impact points (Fig. 8*b*) or very rare, short, shallow and restricted to a few isolated grains (Fig. 8*d*). Whole surface mechanical twinning was not observed at distances equal to or greater than either 21.5 cm in the large grain 50 g charge series, or 27 cm in the large grain 100 g charge series, or 27 cm in the small grain 100 g charge series. Immediately below these thresholds, mechanical twins were just noticeable, but still extended to all surface grains (Fig. 8*e*). Above the threshold, only rare isolated modifications were observed.

In the cross sections, the twinned layer's maximum thickness, which was up to 2 mm in a 6.5 cm distance specimen, rapidly decreased with increasing distance. Not even a partially continuous layer was observed at distances equal to or greater than either 13.5 cm in the large grain 50 g charge series, or 20 cm in the large grain 100 g charge series, or 17 cm in the small grain 100 g charge series (only a few isolated, short and shallow twins, as in Fig. 8*d*, were observed above these thresholds).

At the smallest reduced distances ($r < 0.2$ m/kg$^{1/3}$), mechanical twins were observed, in the cross sections, also close to the opposite face (not directly exposed to the explosion); there was no continuity between these regions and the twinned layer at the ex-

TABLE 3—*Results of the large grain, 50 g charge experimental series.*

No.	d (cm)	Reduced distance (TNT eq.) (m/kg$^{1/3}$)	P_r Computed* (MPa)	P_r Interpolated† (MPa)	τ_{max} (MPa)	Deformation (thickness reduction) (mm)	(%)	Twins (OM) Surface	Section
8	6.5	0.17	158.4			− 0.05	− 1.6	‡	Yes
22	6.5	0.17	158.4			− 0.04	− 1.3	Yes	Yes
12	7.5	0.20	130.0			0	0.0	Yes	Yes
23	8.5	0.22	108.9			− 0.02	− 0.7	Yes	Yes
10	9.5	0.25	92.8			− 0.01	− 0.3	Yes	Yes
30	11.5	0.30	69.4	45.6	23.5	0	0.0	Yes	Yes
2	13.5	0.36	45.0	38.6	19.9	0	0.0	Yes	No
25	16.5	0.44	26.6	31.5	16.2	0	0.0	Yes	No
19	19.5	0.51	17.5	26.5	13.7	0	0.0	Yes	No
13	21.5	0.57	13.8	24.0	12.4	0	0.0	No	No
6	41.5	1.09	3.1			0	0.0	No	No
9	81.5	2.15	0.5			0	0.0	No	No

*Reflected pressure (Eq. 2) on the basis of Henrych formulas (Eq. 1).
†Reflected pressure on the basis of experimental results (Eq. 3).
‡Not observable owing to surface fusion.

TABLE 4—*Results of the large grain, 100 g charge experimental series.*

No.	d (cm)	Reduced distance (TNT eq.) (m/kg$^{1/3}$)	P_r Computed* (MPa)	P_r Interpolated† (MPa)	τ_{max} (MPa)	Deformation (thickness reduction) (mm)	Deformation (thickness reduction) (%)	Twins (OM) Surface	Twins (OM) Section
17	12	0.25	92.5			0.04	1.3	Yes	Yes
18	14	0.29	74.0			0.02	0.6	Yes	Yes
4	17	0.36	45.1	38.7	19.9	0.01	0.3	Yes	Yes
20	20	0.42	29.4	32.7	16.9	0.0	0.0	Yes	No
3	22	0.46	23.1	29.7	15.3	0.0	0.0	Yes	No
21	24	0.50	18.6	27.2	14.0	0.0	0.0	Yes	No
24	27	0.57	13.9	24.1	12.4	0.0	0.0	No	No
7	42	0.88	5.3	15.4	7.9	0.0	0.0	No	No

*Reflected pressure (Eq. 2) on the basis of Henrych formulas (Eq. 1).
†Reflected pressure on the basis of experimental results (Eq. 3).

posed surface. Such a phenomenon, already observed by Tardiff et al. (11) in pure iron, cannot be easily explained without hypothesizing effects of multiple local reflections of the shock wave at the rough free surface.

SEM observations yielded similar results. It has to be noted that OM allows resolution of twins at low magnifications more easily than SEM, because the reflections from tilted and untilted crystal zones allow a clear distinction in the optical microscope, whereas the elevation differences between tilted and untilted crystal zones, observable in the SEM, were less evident. SEM micrographs, on the other hand, provide better detail identification at higher magnifications. Figures 9*a* and *b* show in effect that SEM is important at high magnifications only. For the above reasons, OM is the more suitable tool for large area observation, whereas SEM is most applicable after twins have been singled out in a sample by OM.

Tables 3–5 summarize the experimental results. The occurrence of mechanical twinning both upon the whole exposed surface and in the section (in the mostly limited layer adjacent to the exposed boundary) is listed. As twinning is the result of an applied resolved shear stress, the maximum surface shear stresses previously reported in Fig. 5 are also listed for distances where overall deformation does not occur, up to the validity limit of the interpolating equation (Eq. 3).

Observability Thresholds

The hypothesis of validity of the elasticity theory, while not applicable at the shortest distances, may be considered to hold near the distance of the OM twins observability threshold; thus, in Table 5, computed maximum shear stresses (τ_{max}) at these thresholds are listed for each experimental series. The threshold value for τ_{max} is the same in all cases ($\sim$13 MPa) if computed on the basis of whole surface twinning; to such a stress, a reduced distance of about 0.55 m/kg$^{1/3}$ corresponds.

Hardness

Specimens' hardness was measured before and after the explosions. In the latter case, measurements were performed upon the exposed surfaces, far away from either fusion or fragment impact areas. In some cases, a measurement was not possible because no area was free of these surface alterations. A limited hardness increase from 115 $HV_{0.1}$ (measured upon as fabricated specimens) up to 136 $HV_{0.1}$ was detected in specimens exposed to blast waves with charge-to-target distances lower than 10 or 18 cm, respectively, for 50 and 100 g charges. The increase was generally larger for specimens subjected to higher pressures.

STM Analysis

The exposed surfaces were investigated by STM using a Topometrix instrument with a 23 × 23 μm scanner and $\sim$1 nm spatial resolution. The working parameters were 1 nA constant current, 33 μm/s scanning speed, and 23 × 23 μm^2 scanning area. The peak-valley height of the surface relief was about $\sim$2 nm upon as-prepared specimens (Fig. 10*a*), and increased after explosions (Fig. 10*b*). The relief due to material protrusion on the blast-exposed surfaces is interpreted as ridges produced during mechanical twinning; thus, the distance between two peaks is correlated to the distance between the twinning planes. Peak

TABLE 5—*Results of the small grain, 100 g charge experimental series.*

No.	d (cm)	Reduced distance (TNT eq.) (m/kg$^{1/3}$)	P_r Computed* (MPa)	P_r Interpolated† (MPa)	τ_{max} (MPa)	Deformation (thickness reduction) (mm)	Deformation (thickness reduction) (%)	Twins (OM) Surface	Twins (OM) Section
A02	10	0.21	120.0			0	0.0	Yes	Yes
A16	12	0.25	92.5			0.03	1.0	Yes	Yes
A17	14	0.29	74.0			0.02	0.7	Yes	Yes
A01	17	0.36	45.1	38.7	19.9	0.01	0.3	Yes	No
A05	20	0.42	29.4	32.7	16.9	0.0	0.0	Yes	No
A04	22	0.46	23.1	29.7	15.3	0.0	0.0	Yes	No
A14	24	0.50	18.6	27.2	14.0	0.0	0.0	Yes	No
A15	27	0.57	13.9	24.1	12.4	0.0	0.0	No	No
A07	32	0.67	9.4	20.3	10.4	0.0	0.0	No	No

*Reflected pressure (Eq. 2) on the basis of Henrych formulas (Eq. 1).
†Reflected pressure on the basis of the experimental results (Eq. 3).

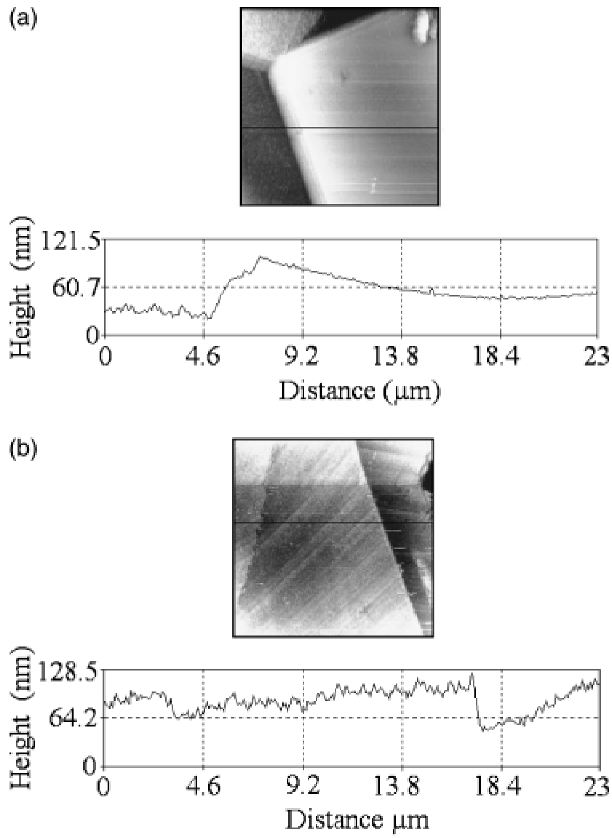

FIG. 10—*Scanning tunneling microscopy images with correspondent line profiles; large-grain specimens, as-prepared (a), submitted to explosions (b) with 50 g charge at 9.5 cm distance (specimen #10).*

heights are due to the displacements connected to twinning process.

Despite a significant variability among points for each specimen, it may be concluded that the average peak-valley height increases with increasing charge and diminishing charge-to-specimen distance, due to increasing applied pressure. In the large-grain, 50 g charge series, the average height diminishes from 20 nm at 9.5 cm distance to 4 nm at 41.5 cm distance. No further variations were observed at larger distances. In the large-grain, 100 g charge series, the same parameter varies from 25 nm at 17 cm distance to 10 nm at 42 cm distance.

The thickness of mechanical twins determined as the distance between successive surface relief features is 250 nm ca. It may be concluded that STM is a very powerful tool to distinguish very fine mechanical twins. It needs a polished original surface to be totally effective as a quantitative measure.

X-Ray Diffraction (XRD) Analysis

Measurement and Calculation—XRD analysis was performed with Mo-K$_\alpha$ ($\lambda = 0.071$ nm) radiation. Overall spectra (5°–60° 2Θ angular range, 0.05° steps and 2 s/step counting time) and precision peak profiles of the {111}, {200}, {220}, {311}, and {331} reflections (0.005° and 10 s/step) were collected in order to identify modifications regarding phases, dislocation density, frequency of mechanical twins and texture before and after the explosions. In the specimens whose surfaces were not wholly twinned, twin-rich regions could nevertheless be found around fragment impact points. Because the XRD analysis involved a large part of the surface, it yielded an average of those regions that were impact

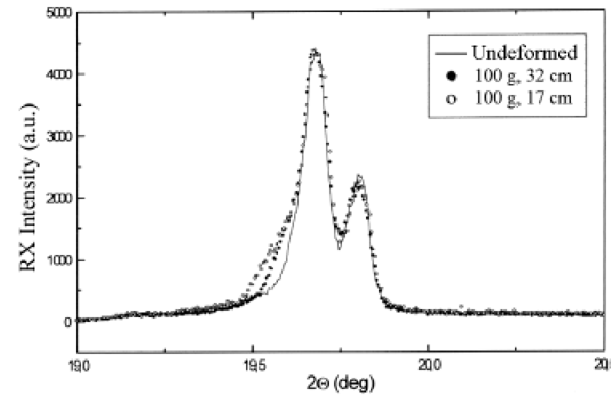

FIG. 11—*Small-grain specimens. X-ray diffraction precision {111} peak profiles of the as-prepared sample and of two samples submitted to explosion with a charge of 100 g at a distance of 17 cm (specimen A1) and of 32 cm (specimen A7). The peak intensities are normalized.*

related and of those that were not. Thus, the XRD analysis is expected to present a greater variability of results with respect to the OM analysis. The latter enables to distinguish local impact-related effects from generalized ones.

The densities of dislocations (ρ), of twin planes (β), and of stacking faults (α) were determined from the analysis of the precision peak profiles, using the following methods. Through Fourier analysis of several XRD precision profiles of deformed and undeformed material, it is possible to separate and determine the contributions to peak broadening of microstrain ε and coherently diffracting domain size D. As microstrains are substantially caused by dislocation structures, the dislocation density ρ can be calculated by the following expression proposed by Williamson and Smallman (12):

$$\rho = \frac{\chi \varepsilon^2}{F b^2} \tag{5}$$

where χ is a parameter connected to microstrain distribution ($\chi = 16.1$), F is a factor depending on dislocation interaction ($F \approx 1$) and b is the length of the Burgers vector ($b = 0.254$ nm).

According to the method reported by Warren (13), the microtwin density β has been determined from the peak asymmetry:

$$\beta = \frac{\sqrt{3}\pi x_2 (y_1 - y_2)}{2A} \left\{ 1 + \left[\frac{\lambda}{4\pi D(\sin\theta_2 - \sin\theta_0)} \right]^2 \right\} \tag{6}$$

TABLE 6—*Threshold distances for detection of explosion-related modifications and corresponding calculated τ_{max} at the specimen surface.*

	Whole-Surface Twinning		Section Layer Twinning	
	Distance (cm)	τ_{max}* (MPa)	Distance (cm)	τ_{max}* (MPa)
60 μm–50 g				
Observed	19.5	13.7	11.5	23.5
Not observed	21.5	12.4	13.5	19.9
60 μm–100 g				
Observed	24	14.0	17	19.9
Not observed	27	12.4	20	16.9
32 μm–100 g				
Observed	24	14.0	14	24.4†
Not observed	27	12.4	17	19.9

*Values calculated (Eq. 4) from experimental interpolated reflected pressure (Eq. 3).
†Value calculated from experimental extrapolated reflected pressure.

The peak ordinates y_1 and y_2 are taken at the same distance x_2 in opposite directions from θ_0, the peak center. D is the grain size, A the area under the peak and θ_2 the angle corresponding to y_2.

The value of β critically depends on the difference $(y_2 - y_1)$; as the difference is usually small, the error is relatively large (±20%). The method is useful to obtain an estimation of microtwin density.

In FCC metals, Paterson's method (14) permits to determine the stacking fault probability α, i.e., the fraction of slip planes affected by faults, from the opposite shifts of two close XRD reflections, in the present case {111} and {200}, using the relationship:

$$\alpha = -\Delta(2\vartheta_{200} - 2\vartheta_{111})^\circ(\pi^2/45\sqrt{3})(0.5\tan\vartheta_{111} + \tan\vartheta_{200})^{-1} \quad (7)$$

where tan is the tangent function and $\Delta(2\vartheta_{200} - 2\vartheta_{111})^\circ = (2\vartheta_{200}–2\vartheta_{111})^\circ_F–(2\vartheta_{200}–2\vartheta_{111})^\circ_U$ is the difference between the angular distance of {200} and {111} peaks in faulted and unfaulted material.

XRD Results

In all examined specimens, XRD spectra showed the γ phase only, while peaks of the ε and α′ martensitic phases were never detected. Further, XRD spectra did not show remarkable variations of the relative peak intensities in samples subjected to explosions under different conditions: the {111} reflection was always the most intense and relative variations lower than 30% were observed in the other reflections. It was not possible to find a sound correlation between these intensity variations and the test parameters (charge and sample–charge distance). The results indicate that experimental tests do not induce strong texture changes in the samples.

As AISI 304Cu has a low stacking fault energy, one would expect to find the presence of stacking faults in the deformed samples, but the absence of peak position shifts showed that their density does not increase appreciably after explosions (15).

Relevant information comes from the examination of peak profiles, which display an asymmetric broadening in particular in the lower part of the peaks and along the tails. This peak asymmetry, a typical effect of mechanical twins on the diffraction pattern (13), increases with increasing explosive charge and decreasing charge-to-specimen distance, i.e., increasing maximum applied pressure. For the same charge and charge-to-specimen distance, specimens with lower grain size showed more asymmetric peaks, indicating more twinning.

An example is reported in Fig. 11, showing the {111} peaks of the as-prepared material and of two small grain samples submitted to explosions with a charge of 100 g at 17 and 32 cm, respectively (specimens A1 and A7). The peak intensities have been normalized to better compare the profiles. The peak profiles substantially overlay in the higher part whereas in the lower part, those of the deformed samples exhibited a shape broadened towards low angles. The effect was stronger for the lower charge-to-sample distance.

The density of dislocations, calculated by Eq. 5, was about $10^8\,\mathrm{cm}^{-2}$ in all the investigated samples, without variations subsequent to the explosions. This is evidence that no measurable slip occurs due to the explosion.

Discussion

Observability Limit Calculation

Mechanical twin observability limits as listed in Table 6 indicate that they correspond to a τ_{max} of about 13 MPa at all charges, as well as at both AISI 304Cu grain sizes used. Shear yield stress for mechanical twins, $\tau_{y,tw}$, has been seen to depend on grain size, d, following a Petch–Hall relationship, both in base-centered cubic (16,17) and in FCC (17) alloys; by a shear to normal stress transformation, one can obtain:

$$\sigma_{y,tw} = \sigma_{f,tw} + k_{tw}(d^{-1/2}) \quad (8)$$

where $\sigma_{y,tw}$ is the $\tau_{y,tw}$ equivalent; $\sigma_{f,tw}$ may be defined as the internal friction stress for twinning. $\sigma_{f,tw}$ incorporates the contribution by the respective critical resolved shear stress for twinning, $\tau_{c,tw}$; like $\tau_{c,tw}$, $\sigma_{f,tw}$ did not vary significantly with the temperature or strain rate. Furthermore, because twinning does not involve time-dependent phenomena (such as dislocation motion), k_{tw} does not significantly vary with the strain rate, like its counterpart, k_{sl}, does in the Petch–Hall equation for slip deformation

$$\sigma_{y,sl} = \sigma_{f,sl} + k_{sl}(d^{-1/2}) \quad (9)$$

.

With small charge explosions, which do not cause appreciable deformations in metal solids exposed to their shock waves, one must determine which is the stress parameter to refer to during an analysis. It is clear that, when effects recorded by OM are limited to a few isolated grains and no macroscopic deformation is present, it is not possible to take into account the alloy yield stress or any other parameter determined macroscopically. Friction stresses for slip or twinning could be used, when applicable. Yet, $\sigma_{f,sl}$ and $\sigma_{f,tw}$, and their corresponding shear stresses, $\tau_{f,sl}$ and $\tau_{f,tw}$, are the extrapolation limits of experimental results as the alloy grain size increases up to infinity, which is not the case of the present research. In the present case, it appears more appropriate to refer to $\tau_{c,tw}$, which is the threshold that has to be overcome to generate twinning in a few isolated favorably oriented grains.

In the literature, no suitable $\tau_{c,tw}$ values were found for austenitic stainless steels; however, it is possible to derive approximate values by taking into account some of the γ_{sf} values derived from the literature for these kind of steels. In fact, $\tau_{c,tw}$ is mainly influenced by the stacking-fault energy, γ_{sf}, and decreases as the latter decreases; austenitic stainless steels are among the alloys with the lowest values of γ_{sf}: 21 mJ/m^2 for AISI 304–316 steels, 40 mJ/m^2 for AISI 310 steel (14) and 11 mJ/m^2 for Mn–Cr austenitic stainless steel (18).

An approximate relation between $\tau_{c,tw}$ and γ_{sf} is derived from that advanced by Suzuki and Barrett (19), omitting a term becoming infinitesimal when the distance among the dislocations increases:

$$\tau_{c,tw} = \gamma_{sf}/2b_1 \quad (10)$$

where $b_1 = a_o/\sqrt{6}$ is the Burgers vector of the Shockley partial dislocation and a_o is the lattice constant.

Another relation is derived by Remy and Pineau (20):

$$(1/\sqrt{3})(1/3 + k\tau_{c,tw}/G)\tau_{c,tw}/G = \gamma_{sf}/G\,\mathrm{b} \quad (11)$$

where $b = a_o\sqrt{2}/2$ is the Burgers vector of a perfect dislocation, G is the shear modulus and k is a fitting coefficient (assumed to be equal to 700 by Remy and Pineau).

Finally, a perfect linear correlation can be traced with γ_{sf} in ordinate and the $\tau_{c,tw}$ in abscissa and plotting data for every FCC metal for which the pertaining γ_{sf} and $\tau_{c,tw}$ values are available in the literature, as proposed by Firrao et al. (1). The straight line derived passes through the origin and its angular coefficient is 0.452 nm. Then, unknown $\tau_{c,tw}$ values can be easily calculated from known γ_{sf} data as

$$\tau_{c,tw} = \gamma_{sf}/0.452 \tag{12}$$

(where $\tau_{c,tw}$ and γ_{sf} are expressed in MPa and in mJ/m^2, respectively).

To compute γ_{sf} values for austenitic stainless steels, Rhodes and Thompson (21) proposed

$$\gamma_{sf} = 1.2 + 1.4[\mathrm{Ni}] + 0.6[\mathrm{Cr}] + 17.7[\mathrm{Mn}] - 44.7[\mathrm{Si}] \tag{13}$$

with an error of ± 8 mJ/m^2 (where the wt% of each alloying element is indicated by its chemical symbol).

Upon introducing into the above formula the exact steel content of Cr, Ni, Mn, and Si, a γ_{sf} value of 21.6 mJ/m^2 is obtained, to which the contribution due to 3.44% Cu has to be added. Choi and Jin (4), basing on computations by Inakazu (22), have evaluated that the presence of 3.21% Cu in these type of steels yields a γ_{sf} increase of 9 mJ/m^2 ca. Then, for the present steel a γ_{sf} value of 31.2 mJ/m^2 can be computed. Moreover, Gonzalez (23) proposes that Cu has an effect on γ_{sf} two times that of Ni. Hence, the above formula in the case of the presence of Cu becomes:

$$\gamma_{sf} = 1.2 + 1.4[\mathrm{Ni}] + 0.6[\mathrm{Cr}] + 17.7[\mathrm{Mn}] - 44.7[\mathrm{Si}] + 2.8[\mathrm{Cu}] \tag{14}$$

yielding a value of 31.3 mJ/m^2 for the present steel.

Thus, a γ_{sf} value of 31 ± 8 mJ/m^2 can be considered appropriate for the present steel.

At such a value of γ_{sf}, Eq. 12 yields a $\tau_{c,tw}$ value equal to 69 MPa. Larger values were obtained using the other two relationships (Eqs. 10 and 11).

$\tau_{c,tw}$ has to be compared with maximum shear stresses due to peak pressures of shock waves. As they decreased, smaller spacings between faults on {111} planes in low γ_{sf} materials were induced. An increase in pulse duration caused larger volumes of twins and martensite (when the martensitic transformation occured) in low-γ_{sf} metals (24). Thus, peak pressure is the dominant parameter in determining the microstructure where strain is small or nonexistent, as in the cases examined in the present research.

The computed τ_{max} applied at the surface of specimens in correspondence of the optical microscopy observability limit of surface twins was determined as being 13 MPa, much lower than computed $\tau_{c,tw}$. Even adopting the minimum acceptable value of γ_{sf} (23 mJ/m^2 from Eq. 13 where the copper contribution was not considered), a $\tau_{c,tw}$ equal to 51 MPa could be determined (from Eq. 12), still much larger than the computed τ_{max} values.

The influence of other effects besides the peak pressure has to be taken into account to fully understand the twinning phenomenon in metals under exploding charges and to devise a precise procedure to foresee the maximum charge-to-target distance at which mechanical twins are still visible by OM from physical calculations. A sizable contribution to shear stresses may come from the constrained dilatation originating on the upper portion of the specimens from the temperature wave, which rapidly dissipates within the samples at the distances corresponding to the observability limits. Research is continuing to further explore the issue.

Metal Objects Mapping in an Explosion

For forensic science purposes, austenitic stainless-steel objects showing mechanical twins can be easily placed on a map of the small charge explosion location using the experimentally determined observability limits listed in Table 6, which yielded a free-field reduced distance radius of about 0.55 m/kg$^{1/3}$ for whole surface twinning due to the reflected pressure. Useful indications about the charge mass may also be obtained by observing surface damage and measuring macro-deformations; the latter were not detected at a reduced distance above about 0.27 m/kg$^{1/3}$ for 54.5 g TNT-equivalent charges and of about 0.40 m/kg$^{1/3}$ for 109 g TNT-equivalent charges.

If objects with only a few twinned crystals at the exposed surfaces are identified, they can be thought as being on the surface of a sphere with a reduced distance radius slightly larger than 0.55 m/kg$^{1/3}$. Then, if two stainless-steel objects with very few twins are found and their original position established, the charge position, if unknown, can be identified by drawing two spheres centered at the object locations with radius equal to $0.55m^{1/3}$ m (m is the hypothesized charge mass in kilograms). The charge will be located on the circumference, which is the intersection of the two spherical surfaces.

Also, if m is unknown, a reasonable hypothesis about the charge mass can be obtained by taking into account the distance, d, between the two twinned metal objects centers; the value of m has to allow that $1.10m^{1/3}$ is equal to or greater than d.

If more than two objects are found, the charge can be located more precisely. Topographical considerations may help in singling out explosive location or mass.

This approach yielded useful results in a criminal case, involving a small aircraft destroyed by an on-board bomb in 1962. The case, originally considered as an accident, was recently re-opened and it was possible to ascertain that an explosion occurred and to estimate the bomb's position (25), by analyzing the only few metal objects that were inside the cockpit and had remained available, namely a cockpit instrument and a ring of a passenger riding in the front passenger seat (the other aircraft's remnants had been disposed of after the first investigation).

The presence of screens of various nature between charge and target may alter the picture, the amount of energy dissipation induced by them depending on the material, the shape, the thickness and the position of the screen. Further tests with screens, made with selected materials and having different shape and thickness, are needed to obtain quantitative results in this respect, along with numerical simulations.

The whole picture can be further altered if the explosion wave propagates in a confined space; multiple reflections can increase the observability limits above those listed in Table 6.

Conclusions

A series of explosions of small 50 and 100 g charges made of NSP Bofors Nobelkrut D UN N.0084 explosive (TNT equivalents, 54.5 and 109 g) were performed close to stainless-steel targets. The charge-to-target distances were in the 6.5–81.5 cm range. The targets were 3-mm-thick disks of AISI 304Cu austenitic stainless steel, with 60 and 32 μm average grain sizes. It has been possible to ascertain the following aspects:

i. Only at the shortest distances (up to 10 cm) fusion of the surfaces may occur.
ii. Macroscopic deformations are very limited and dissipate above a 10 cm distance for samples tested with NSP 50 g charges or at 18 cm for samples in NSP 100 g explosions. The respective reduced distances ($r = dm^{-1/3}$) are 0.27 and 0.40 m/kg$^{1/3}$.
iii. Crystal structure alterations mainly consist of extensive formation of mechanical twins close to the exposed surface,

with very limited surface recrystallization at the shortest distances. At these distances, twins occupy a good portion of the section, but never the entire thickness; they may also appear in a very limited layer bordering the opposite free surface.

iv. Twinning has been observed by optical and scanning electron microscopy, STM and XRD. The former is considered the most reliable easy-to-use observation method. No effect was observed on the surface for charge-to-target distances larger than 21.5 cm in the 60 μm average grain size 50 g charge series or larger than 27 cm in the 60 and 32 μm 100 g series. The reduced distance observability threshold for whole-surface twinning was the same in all cases: about 0.55 m/kg$^{1/3}$.

v. Using a series of tests with sensor instrumented targets, explosion peak pressures were measured and related to the maximum shear stresses, τ_{max}, applied at the specimens' surface when postexplosion macro-deformation was absent. The τ_{max} value computed at the limiting optical microscopy observability distance was equal for all the adopted experimental conditions (13 MPa) and was compared with the critical resolved shear stress for twinning, $\tau_{c,tw}$, which was much higher.

vi. To explain such a difference, other effects, like constrained surface dilatation due to temperature waves rapidly disappearing in the bulk, have to be taken into account.

vii. For forensic science purposes, austenitic stainless-steel objects showing mechanical twins can be located on a map of an explosion within a reduced distance of about 0.55 m/kg$^{1/3}$. Using of such an observability limit, metal objects of this kind can be used to help locate the explosive charge or to identify the charge mass.

Acknowledgments

This work was financially support of the Italian Ministry of Education, University, and Research, by the "Progetto di Rilevante Interesse Nazionale #2001094974."

References

1. Firrao D, Ubertalli G, Cordano E. Was it a bomb? A reply from the microscope. Technol, Law Insur 1999;4:23–30.
2. Dieter GE. Hardening effects produced with shock waves. In: Harwood JJ, editor. Strengthening mechanisms in solids. Proceedings of a seminar of the American Society for Metals; 1960 October 13–14. Metals Park, OH: American Society for Metals; 1962:279–340.
3. Meyers MA, Chawla KK. Mechanical metallurgy: principles and applications. Englewood Cliffs, NJ: Prentice-Hall; 1984.
4. Choi JY, Jin W. Strain induced martensite formation and its effect on strain hardening behavior in the cold drawn 304 austenitic stainless steels. Scripta Mater 1996;36:99–104.
5. Henrych J. The dynamic of explosion and its use. Amsterdam: Elsevier; 1979.
6. Petralia S. Compendio di esplosivistica. La Spezia: MARIPERMAN; 2000.
7. Esparza ED. Blast measurements and equivalency for spherical charges at small scaled distances. Int J Impact Eng 1986;4:23–40.
8. Ismail MM, Murray SG. Study of the blast wave parameters from small scale explosions. Propellants Explosives Pyrotechnics 1993;18:11–7.
9. Brandes EA, Brook GB, editors. Smithells metals reference book. Oxford: Butterworth-Heinemann; 1992:14–35, 15–3.
10. Firrao D, Matteis P, Scavino G, Ubertalli G, Ienco MG, Piccardo P, et al. AISI 304Cu steel subjected to small charge explosions: microstructural changes with limited or no macro-deformation. In: Schlesinger ME, editor. EPD Congress 2005; 13–17 Feb 2005. San Francisco, USA: TMS; 2005.
11. Tardiff HP, Claisse F, Chollet P. Some observations in explosively loaded iron and mild steel. In: Shewmon PG, Zackay VF, editors. Response of metals to high velocity deformation. New York, USA: Interscience; 1961.
12. Williamson GK, Smallman RE. Dislocation densities in some annealed and cold-worked metals from measurements on the X-ray Debye–Scherrer spectrum. Philos Mag 1956;1:34–45.
13. Warren BE. X-ray diffraction. Reading, MA, USA: Addison Wesley Publishing Company; 1969:288.
14. Kestenbach HJ. Effect of applied stress on partial dislocation separation and dislocation substructure in austenitic stainless steel. Philos Mag 1977;36:1509–15.
15. Paterson MS. X-ray diffraction by face-centered cubic crystals with deformation faults. J Appl Phys 1952;23:805–11.
16. Armstrong RW, Worthington PJ. A constitutive relation for deformation twinning in body centered cubic metals. In: Rohde RW, Butcher BM, Holland JR, Karnes CH, editors. Metallurgical effects at high strain rates. New York, USA: Plenum Press; 1964:401–14.
17. Meyers MA, Vöhringer O, Lubarda VA. The onset of twinning in metals: a constitutive description. Acta Mater 2001;49:4025–39.
18. Remy L, Pineau A. Twinning and strain-induced FCC-HCP transformation in the Fe–Mn–Cr–C System. Mater Sci Eng 1977;28:99–107.
19. Suzuki H, Barrett C. Deformation twinning in silver–gold alloys. Acta Metall 1958;6:156–65.
20. Remy L, Pineau A. Twinning and strain-induced FCC–HCP transformation on the mechanical properties of Co–Ni–Cr–Mo alloys. Mater Sci Eng 1976;26:123–32.
21. Rhodes CG, Thompson AW. The composition dependence of stacking fault energy in austenitic stainless steels. Met Trans A 1977;8A:1901–6.
22. Inakazu N, Yamamoto H, Ishio M. On the development of deformation and transformation textures during cold drawing in austenitic stainless steels. J Jpn Inst Met 1984;48:71–8.
23. Gonzalez BM, Castro CSB, Buono VTL, Vilela JMC, Andrade MS, Moraes JMD, et al. The influence of copper addition on the formability of AISI 304 stainless steel. Mater Sci Eng A 2003;343:51–6.
24. Murr LE. Interfacial phenomena in metals and alloys. Reading, MA, USA: Addison-Welsey; 1975:145–7.
25. Calia V. Richieste del Pubblico Ministero, Procedimento Penale n. 181/84 mod. 44, Procura della Repubblica presso il Tribunale di Pavia, Pavia (Italy), February 20, 2003.

Additional information and reprint requests:
Donato Firrao, M.Sc.
Dipartimento di Scienza dei Materiali ed Ingegneria Chimica
Politecnico di Torino
Corso Duca degli Abruzzi 24
10129 Torino
Italy
E-mail: donato.firrao@polito.it